Communication

Agglomeration of Solid Inclusions in Molten Steel

HAOJIAN DUAN, YING REN,
BRIAN G. THOMAS, and LIFENG ZHANG

Agglomeration of alumina inclusions in the molten steel is investigated through the free energy analysis of the cavitation between inclusions. The mechanism of agglomeration, the activation state, the stable state, the equilibrium state, and the critical separation for the cavitation are discussed. The equilibrium energy is proportional to the square of the inclusion radius, $E_{Eq} = 0.710R_P^2$, while the critical separation is directly proportional to the inclusion radius, $d_C = 0.146R_P$. Agglomerates of micron inclusions are hardly broken up by the turbulence in steelmaking practice.

https://doi.org/10.1007/s11663-018-1478-2

Agglomeration of solid particles in liquid is relevant to numerous commercial products and industrial processes,[1] such as metallurgical engineering,[2,3] materials fabrication,[4,5] and pharmaceuticals.[6] During the steelmaking process, deoxidizer is added into the molten steel and inclusions are generated during the deoxidation production through the reaction between the deoxidizer and the dissolved oxygen.[7] Fine inclusions can grow rapidly through agglomeration and coalescence. Nevertheless, large clusters in the steel are detrimental to the mechanical properties and can easily deposit on the submerged entry nozzle, causing clogging.[8,9] Thus, understanding the agglomeration mechanism of inclusions in molten steel is of great importance for predicting and controlling inclusion behavior and steel cleanness. Generally, solid inclusions are nonwetted in the molten steel (the contact angle exceeds 90 deg), such as 136 deg for alumina inclusions[10] and 102 deg for silica inclusions.[11] Agglomeration easily occurred among those inclusions to form clusters. Figure 1 shows the example of the agglomeration of alumina inclusions in interstitial-free (IF) steel.

Recently, the cavitation theory[12–15] that the liquid spontaneously expelled from the gap between solid particles to form a cavity as the solid particles approach each other was used to explain the agglomeration of inclusions in the molten steel. Sasai[16,17] established an experimental method to directly measure the agglomeration force exerted between alumina inclusions in molten steel and to evaluate the formation and extinction behavior of cavity bridges between alumina inclusions. It was demonstrated that the agglomeration force is derived from the cavity bridge force. Zheng *et al.*[18] investigated the effect of alumina morphology on the clustering behavior by analyzing the attractive force between two alumina inclusions with different shapes in molten steel based on the cavitation theory.

Even though the agglomeration of solid inclusions in the molten steel due to the cavitation was reported previously,[16–18] many details regarding this phenomenon still need to be further clarified. The current study investigated the formation and the stability of the cavity between solid inclusions from the view of free energy analysis based on the bridge cavitation theory. Several key parameters for the agglomeration, such as the equilibrium energy and the critical separation, were proposed and discussed. The agglomeration mechanism was proposed through the free energy analysis of the cavitation. Experimental results reported by Sasai[16,17] were used for comparison to validate the model. The effect of the turbulence on the agglomeration of inclusions was discussed.

When two solid inclusions approach each other in the molten steel with a narrow space, a gas cavity is formed between inclusions due to the poor wettability, as shown in Figure 2. The profile of the meniscus (gas–liquid interface) can be approximated by a circular arc. The curvature radius of the meniscus and the radius of the cavity at its neck are obtained from the geometrical relationship as a function of the filling angle, β:

$$R_M = -\frac{R_P(1-\cos\beta)+d/2}{\cos(\theta-\beta)} \quad [1]$$

$$R_N = R_P\sin\beta - R_M[1-\sin(\theta-\beta)] \quad [2]$$

where R_P, R_M, and R_N are the radius of inclusions, the meniscus radius, and the neck radius, respectively; d is the separation between inclusion surfaces along their axis; and θ is the contact angle between inclusions and the molten steel.

Then, the areas of the inclusion-cavity interface and the liquid-cavity interface are given by

$$S_{SC} = 2\pi R_P^2(1-\cos\beta) \quad [3]$$

HAOJIAN DUAN, YING REN, and LIFENG ZHANG are with the School of Metallurgical and Ecological Engineering, University of Science and Technology Beijing (USTB), Beijing 100083, China. Contact emails: renyingfour@163.com; zhanglifeng@ustb.edu.cn BRIAN G. THOMAS, is with the Department of Mechanical Engineering, Colorado School of Mines, Golden, CO 80401

Manuscript submitted September 15, 2018.
Article published online January 2, 2019.

$$S_{LC} = 4\pi R_M \left[(R_M + R_N) \arcsin \frac{R_P - R_P \cos\beta + d/2}{R_N} - (R_P - R_P \cos\beta + d/2) \right] \quad [4]$$

The volume of the cavity is obtained by integrating the following equation:

$$V = 2\pi \int_0^{R_P - R_P \cos\beta + d/2} \left[(R_M + R_N) - \sqrt{R_M^2 - x^2} \right]^2 dx - \frac{2\pi}{3} R_P^3 (\cos^3\beta - 3\cos\beta + 2) \quad [5]$$

Based on the theory of interfacial chemical interactions, the free energy change during inclusion approaching is considered to involve three parts:

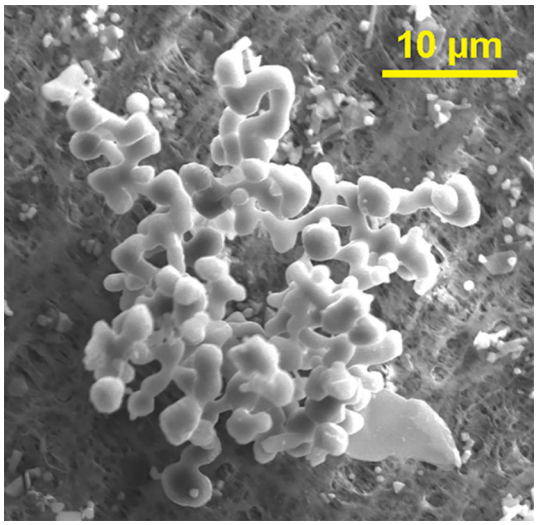

Fig. 1—Agglomeration of alumina inclusions in IF steel.

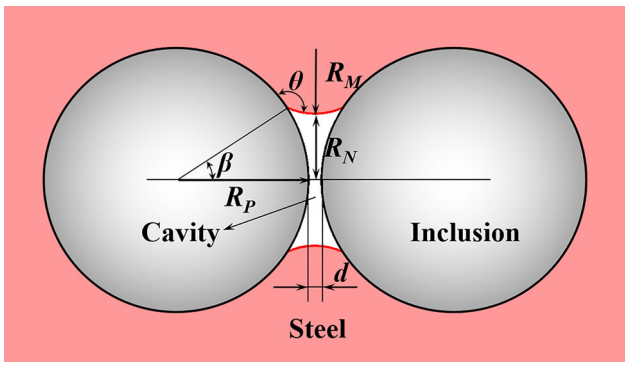

Fig. 2—Schematic of cavitation between inclusions.

$$\Delta E = 2S_{SC}(\sigma_S - \sigma_{LS}) + \sigma_L S_{LC} + \Delta pV = 2S_{SC}\sigma_L \cos\theta + \sigma_L S_{LC} + \Delta pV \quad [6]$$

where σ_{LS}, σ_S, and σ_L are the interface tensions between the molten steel and inclusions, the surface tension of inclusions, and the surface tension of the molten steel, respectively, and Δp is the pressure difference across the meniscus. The first term is the free energy change caused by the receding of the molten steel from the gap between inclusion surfaces, which drives the formation of the cavity. The second term is the work spent on the formation of the liquid-cavity interface, and the last is the vapor energy; both of the latter two terms are the resistance of the cavity formation.

Agglomeration of alumina inclusions in the molten steel was taken as an example. The surface tension of the

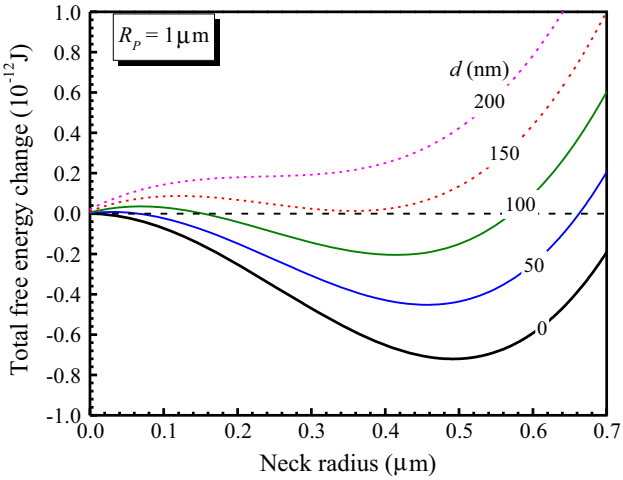

Fig. 3—Total free energy change as a function of neck radius at different separations for alumina inclusions of 1 μm in radius.

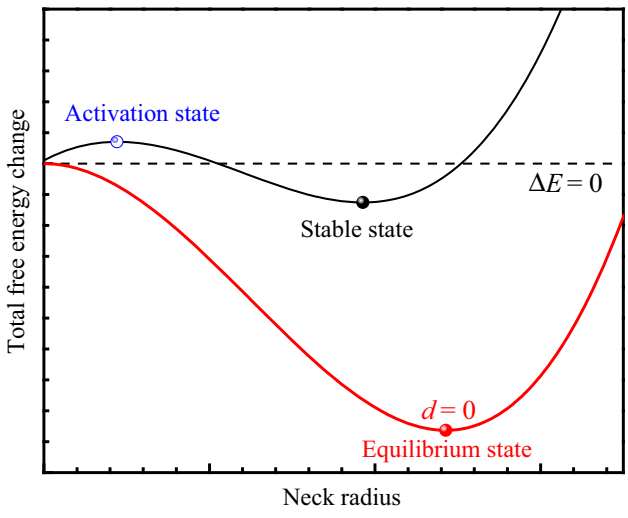

Fig. 4—Definition of activation state, stable state, and equilibrium state.

molten steel and the contact angle of that with alumina inclusions were 1.80 N/m and 137 deg, respectively.[16] Since the pressure inside the cavity is not accurately known at this point,[14,19] the pressure deficiency in this study was set as a constant of 3.86×10^3 Pa according to the experimental results of Sasai.[16] The radius of the alumina inclusions was assumed to be 1 μm. Commercial software Matlab was employed to solve the numerical equations. First, the curvature radius and the neck radius were calculated by using Eqs. [1] and [2] as a function of the filling angle. Then, the area of the inclusion-cavity interface, the area of the liquid-cavity interface, and the volume of the cavity were calculated according to Eqs. [3] through [5]. Finally, the total free energy change is estimated by Eq. [6]. Figure 3 shows the total free energy change as a function of the neck radius at different separations.

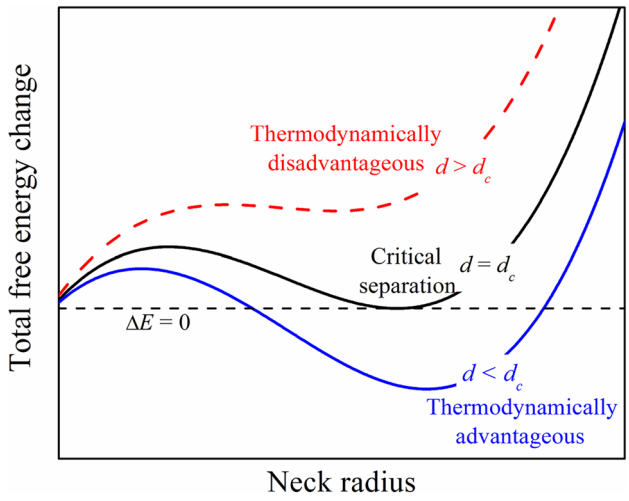

Fig. 5—Definition of critical separation.

In order to clearly explain the cavitation between inclusions, several definitions are proposed. Figure 4 illustrates the typical curve of total free energy change with respect to the neck radius. First, the total free energy change increases with the increase of the neck radius until reaching a local maximum. At the maximum, the system reaches the activation state and the maximum value represents the energy barrier for cavitation. Subsequently, the total free energy change starts to decrease with the neck radius further increasing. The stable state is achieved by minimizing the total free energy with respect to the neck radius when the cavity grows beyond the activation state, as shown in Figure 4.

For the case of inclusions contacting each other, the stable energy reaches the minimum with respect to separation. In the meantime, the system is also at the lowest energy state and, thus, the cavity is at the most stable state. Clearly, once the inclusions move close to a critical separation and the cavity is formed, they will approach each other spontaneously until they contact due to the decrease of the free energy, as shown in Figure 4. Consequently, the ultimate state of the system is achieved as the inclusions contact each other, which can be defined as the equilibrium state. The absolute value of the stable energy is defined as the equilibrium energy.

When a small gap appears between inclusions, the stable energy shows a negative value, indicating that the formation of the cavity is thermodynamically advantageous. However, with further increase in the separation, the stable energy increases beyond zero. At this moment, the formation of the cavity is thermodynamically disadvantageous. Thus, the critical separation is also

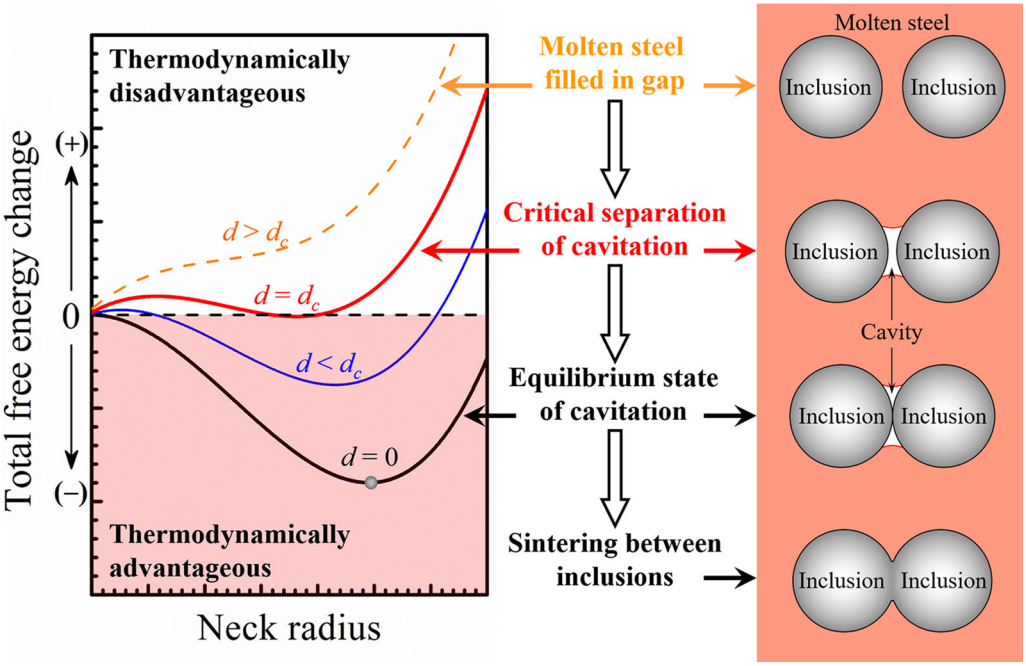

Fig. 6—Agglomeration mechanism of inclusions in molten steel.

achieved as the total free energy change turns into zero during the cavitation between spherical inclusions, as shown in Figure 5. Physically, the cavity can exist between inclusions only for the separation below the critical separation. It should be noticed that there still exists an energy barrier at the critical state. Thus, for the case of separation shorter than the critical separation, the cavity sustains spontaneous growth when the energy barrier has been overcome.

The agglomeration mechanism of solid inclusions in molten steel is proposed according to the free energy analysis, as shown in Figure 6. In the molten steel, the dispersed inclusions approach each other due to their random motion. Once the separation is shorter than the critical separation, the cavity is formed between inclusions when the energy barrier has been overcome. As shown in Figure 3, the system energy decreases during the approach process and the lowest energy state is achieved when the inclusions contact each other. Thus, the inclusions continue to move close to each other spontaneously until contact to achieve the equilibrium state, which is the ultimate state of the cavitation. Sintering occurs between inclusions after the equilibrium state. Future studies will focus on the sintering of solid inclusions in the molten steel, which is the subsequent step after agglomeration.

As discussed previously, two crucial states are observed during cavitation: equilibrium state and critical state. The dependence of equilibrium energy and critical separation on the radius of inclusions is numerically calculated, as shown in Figure 7. It is novel for the present study to find that the equilibrium energy is a quadratic function of the inclusion radius and the critical separation is directly proportional to the radius of inclusions. The regression lines in Figure 7 give the following equations for the equilibrium energy and the critical separation:

$$E_{\mathrm{Eq}} = 0.710 R_{\mathrm{P}}^2 \qquad [7]$$

$$d_{\mathrm{C}} = 0.146 R_{\mathrm{P}} \qquad [8]$$

It can be seen from Figure 7 that numerical calculation results satisfy these equations. The equilibrium energy can be used to judge the conditions for the break up of agglomerates, and the critical separation can provide a criterion for specifying the agglomeration behavior between inclusions.

In order to validate the model, experimental results reported by Sasai[16,17] are used for comparison. For two isodiametric Al_2O_3 cylinders immersed in molten steel, the problem could be simplified into a two-dimensional section model due to the length of the cylinders (50 mm) being much larger than the cylinder surface distance (<1.0 mm). Therefore, the solid-cavity surface area, the liquid-cavity surface area, and the volume of the cavity can be obtained from the following equations, respectively:

$$S_{\mathrm{SC}} = 2\beta R_{\mathrm{P}} \qquad [9]$$

$$S_{\mathrm{LC}} = 4\left(\theta - \beta - \frac{\pi}{2}\right) R_{\mathrm{P}} \qquad [10]$$

$$V = 2\int_0^{R_{\mathrm{P}} - R_{\mathrm{P}}\cos\beta + d/2} \left[(R_{\mathrm{M}} + R_{\mathrm{N}}) - \sqrt{R_{\mathrm{M}}^2 - x^2}\right] \mathrm{d}x - (2\beta - \sin 2\beta) R_{\mathrm{P}}^2 \qquad [11]$$

Similarly, the total free energy change of the cavity formation is expressed as

$$\Delta E = 2S_{SC}\sigma_L \cos\theta + \sigma_L S_{LC} + \Delta p V \qquad [12]$$

Figure 8(a) shows the measured cavitation in the section of 8-mm alumina cylinders with different

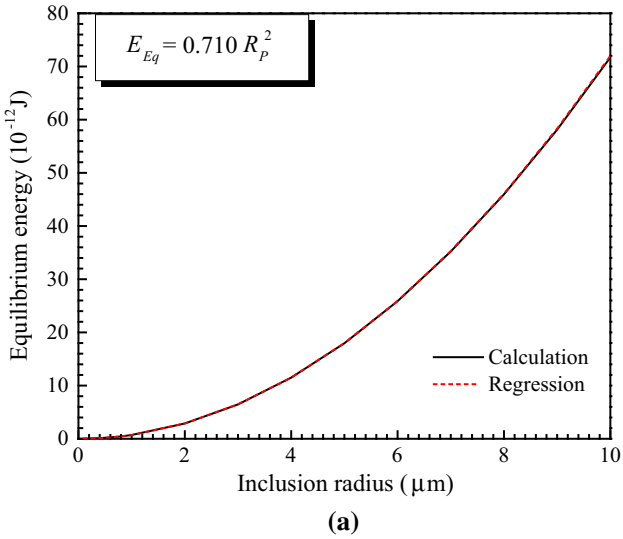

(a)

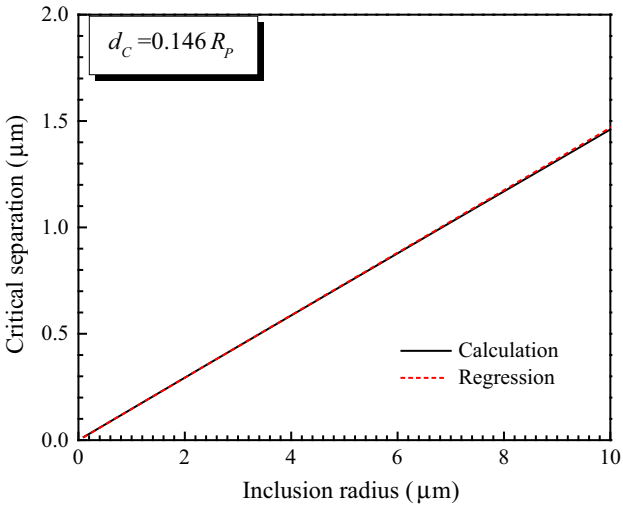

(b)

Fig. 7—(*a*) Equilibrium energy and (*b*) critical separation as a function of inclusion radius.

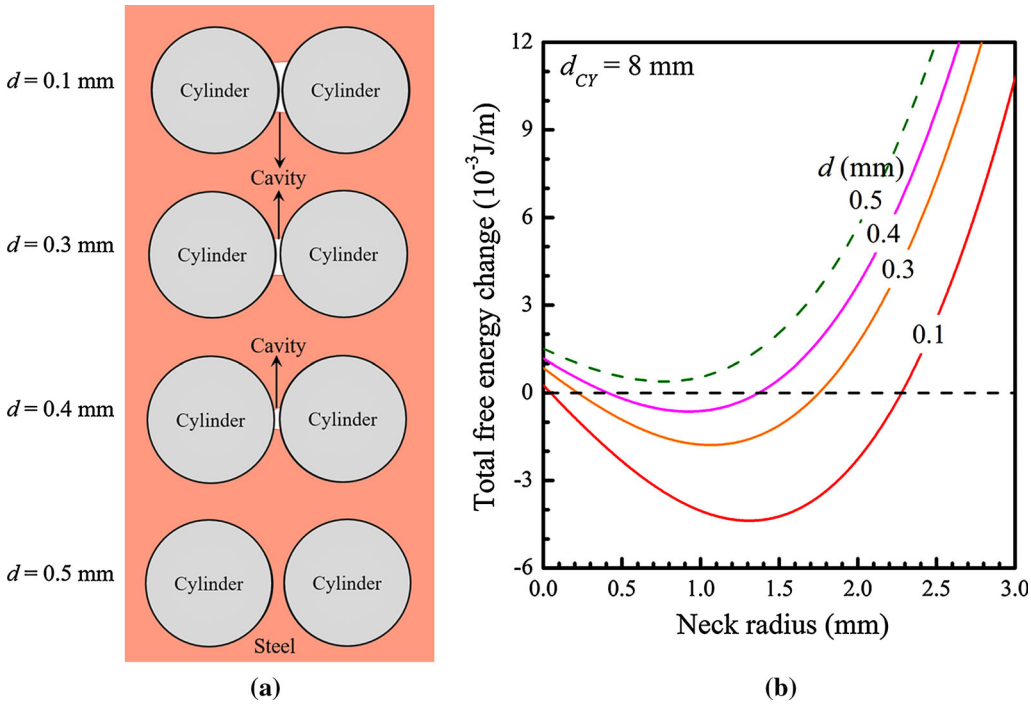

Fig. 8—Cavitation between two 8-mm alumina cylinders in molten steel: (*a*) experimental and (*b*) calculation.

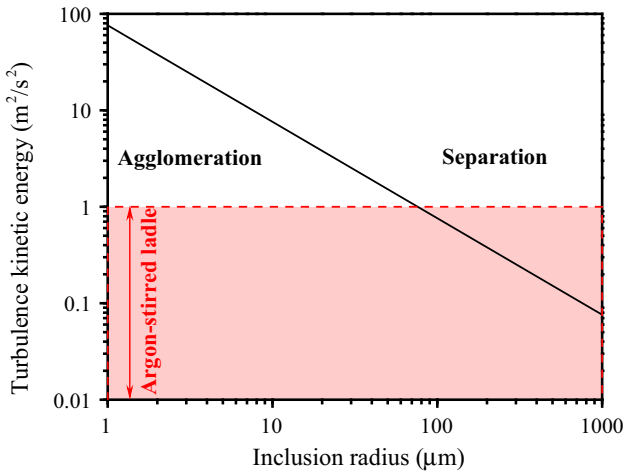

Fig. 9—Effect of local turbulence kinetic energy on inclusion agglomeration.

separations, and Figure 8(b) shows the calculated total free energy change as a function of neck radius for alumina cylinders at different separations. It should be noted that the value of 152.6 deg was used as the contact angle to validate the model since it was reported by Sasai[16,17] in the experiment. Clearly, the cavity is formed for separations below 0.4 mm, while the cavity cannot be formed as the separation increases to 0.5 mm. In Figure 8(b), the stable energy for the cavitation shows a negative value as the separation is shorter than 0.4 mm, indicating that the formation of cavity is thermodynamically advantageous. As the separation increases to 0.5 mm, the stable energy is larger than zero and the cavity hardly forms between cylinders. Moreover, the stable radius decreases with the increase of the separation, which also has been found in the experiment, as shown in Figure 8(a).

The behavior of inclusions in the molten steel is affected by the turbulent fluid flow. The contacted inclusions may break up due to the random motion of the turbulence. It is assumed that the energy induced by the turbulence is the product of the inclusion mass and the local turbulence kinetic energy:

$$E_{\text{inc}} = 2m_{\text{inc}}k = \frac{8}{3}\pi R_{\text{I}}^3 \rho_{\text{inc}} k \qquad [13]$$

where m_{inc} is the mass of the inclusion, k is the local turbulence kinetic energy, ρ_{inc} is the density of the inclusion, and the value of 3500 kg/m^3 is used for alumina.

Physically, the equilibrium energy also represents the lowest energy that should be overcome for the disappearance of cavity between the contacted inclusions. Thus, combining Eq. [13] with the equilibrium energy, the relationship between the turbulence kinetic energy, which could separate the contacted inclusion, and the radius of the inclusions is obtained for Al_2O_3 inclusions, as shown in Figure 9. Obviously, the smaller the inclusions are, the higher the turbulence kinetic energy required to separate them. For micron scale inclusions, the local turbulence kinetic energy required to break up the already contacted inclusions should be larger than 1 m^2/s^2, while for millimeter scale inclusions, the value lies below 0.1 m^2/s^2. During the steelmaking process, the local turbulence kinetic energy hardly reaches 1.0 m^2/s^2 in the molten steel, as shown in Figure 9.[20–22] Thus, the aggregation of the micron-sized inclusions could exist in a stable state and the contacted inclusions are hardly separated by the turbulence.

In the current study, the agglomeration of nonwetted solid inclusions in the molten steel is investigated using the free energy analysis based on the bridge cavitation theory, and the following conclusions have been reached.

(1) The agglomeration mechanism of solid inclusions in the molten steel is proposed: the cavity is generated between two inclusions as the separation reaches the critical separation. After that, inclusions move close to each other spontaneously as a result of the decrease of the free energy. The equilibrium state of the cavitation is achieved when the inclusions contact each other, after which sintering occurs.
(2) The equilibrium state is achieved when the inclusions contact each other. The equilibrium energy is a quadratic function of the inclusion radius. For the agglomeration of alumina inclusions in the molten steel, $E_{Eq} = 0.710R_P^2$.
(3) The critical separation for the cavitation between inclusions is derived, at which the total free energy change turns into zero. The critical separation is linearly proportional to the inclusion radius: $d_C = 0.146R_P$.
(4) In practice, the micron-scaled contacted inclusions can hardly be separated by the turbulence.

The authors are grateful for the support from the National Key R&D Program of China (2017YFB0304000 and 2017YFB0304001), the National Science Foundation of China (Grant No. 51725402), the Beijing Key Laboratory of Green Recycling and Extraction of Metals (GREM), and the High Quality Steel Consortium (HQSC) and Green Process Metallurgy and Modeling (GPM^2), School of Metallurgical and Ecological Engineering, University of Science and Technology Beijing (USTB).

REFERENCES

1. W. Pietsch: *Agglomeration in Industry: Occurrence and Applications*, Wiley, Hoboken, 2008.
2. W. Kim and I. Sohn: *ISIJ Int*., 2011, vol. 51, pp. 63–70.
3. W. Liu, L. Qiu, Z. Wang, Q. Li, X. Ye, and Y. Han: *J. Tsinghua Univ*., 2013, vol. 53, pp. 573–77.
4. A. Realpe, C. Velazquez, and L. Obregon: *AIChE J*., 2009, vol. 55, pp. 1127–34.
5. A.P. Wemhoff and A.J. Webb: *Int. J. Heat Mass Transfer*, 2016, vol. 97, pp. 432–38.
6. D. Amaro-Gonzalez and B. Biscans: *Powder Technol*., 2002, vol. 128, pp. 188–94.
7. L. Zhang, Y. Ren, H. Duan, W. Yang, and L. Sun: *Metall. Mater. Trans. B*, 2015, vol. 46B, pp. 1809–25.
8. W. Yang, H. Duan, L. Zhang, and Y. Ren: *JOM*, 2013, vol. 65, pp. 1173–80.
9. L. Zhang: *JOM*, 2013, vol. 65, pp. 1138–44.
10. K. Nogi and K. Ogino: *Can. Metall. Q*., 1983, vol. 22, pp. 19–28.
11. K. Ogino, A. Adachi, and K. Nogi: *Tetsu-to-Hagané*, 1973, vol. 59, pp. 1237–44.
12. V.V. Yaminsky, V.S. Yushchenko, E.A. Amelina, and E.D. Shchukin: *J. Coll. Interface Sci*., 1983, vol. 96, pp. 301–06.
13. V.S. Yushchenko, V.V. Yaminsky, and E.D. Shchukin: *J. Coll. Interface Sci*., 1983, vol. 96, pp. 307–14.
14. H.K. Christenson and P.M. Claesson: *Science*, 1988, vol. 239, pp. 390–92.
15. R.M. Pashley, P.M. McGuiggan, B.W. Ninham, and D.F. Evans: *Science*, 1985, vol. 229, pp. 1088–89.
16. K. Sasai: *ISIJ Int*., 2014, vol. 54, pp. 2780–89.
17. K. Sasai: *ISIJ Int*., 2016, vol. 56, pp. 1013–22.
18. L. Zheng, A. Malfliet, P. Wollants, B. Blanpain, and M. Guo: *ISIJ Int*., 2016, vol. 56, pp. 926–35.
19. S. Singh, J. Houston, F. Van Swol, and C.J. Brinker: *Nature*, 2006, vol. 442, p. 526.
20. H. Duan, Y. Ren, and L. Zhang: *JOM*, 2018, vol. 70, pp. 2128–38.
21. H. Duan, L. Zhang, B.G. Thomas, and A.N. Conejo: *Metall. Mater. Trans. B*, 2018, vol. 49B, pp. 2722–43.
22. W. Lou and M. Zhu: *Metall. Mater. Trans. B*, 2013, vol. 44B, pp. 1251–63.